RSC Advances

ROYAL SOCIETY OF CHEMISTRY

www.rsc.org/advances

Investigation of charge transport properties in less defective nanostructured ZnO based Schottky diode

Arka Dey[a], Animesh Layek[b], Anirban Roychowdhury[c], Mrinmay Das[a], Joydeep Datta[a], Somnath Middya[d], Dipankar Das[c] and Partha Pratim Ray[a*]

[a]Department of Physics, Jadavpur University, Kolkata – 700 032, India

[b]Department of Physics, Bejoy Narayan Mahavidyalaya, Itachuna, Hooghly-712147, India

[c]UGC-DAE Consortium for Scientific Research, III/LB-8, Bidhannagar, Kolkata-98, India

[d]Department of Physics, Bankim Sardar College,Tangrakhali, South 24-paraganas, pin-743329, India

*Corresponding Author, e-mail:partha@phys.jdvu.ac.in

Phone: +91-9475237259

Fax: +91-3324138917

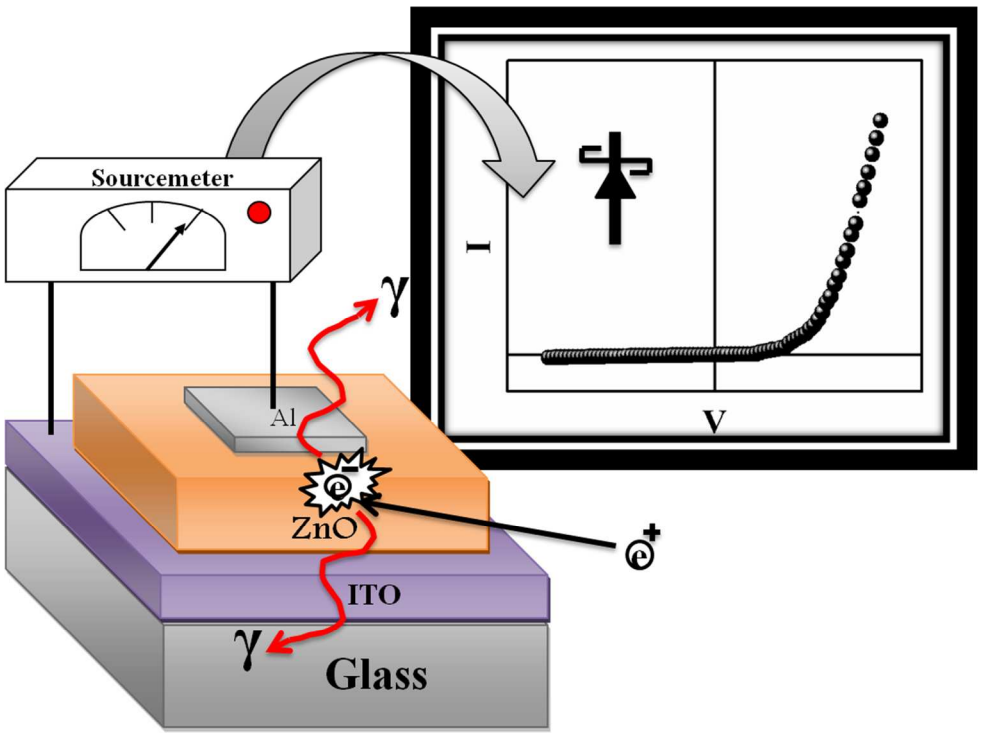

Positron annihilation approved less amount of defect in ZnO: effect on the performance of Al/ZnO/ITO Schottky diode

Investigation of charge transport properties in less defective nanostructured ZnO based Schottky diode

Arka Dey[a], Animesh Layek[b], Anirban Roychowdhury[c], Mrinmay Das[a], Joydeep Datta[a], Somnath Middya[d], Dipankar Das[c] and Partha Pratim Ray[a*]

[a]Department of Physics, Jadavpur University, Kolkata – 700 032, India

[b]Department of Physics, Bejoy Narayan Mahavidyalaya, Itachuna, Hooghly-712147, India

[c]UGC-DAE Consortium for Scientific Research, III/LB-8, Bidhannagar, Kolkata-98, India

[d]Department of Physics, Bankim Sardar College,Tangrakhali, South 24-paraganas, pin-743329, India

*Corresponding Author, e-mail:partha@phys.jdvu.ac.in

Phone: +91-9475237259

Fax: +91-3324138917

Abstract

In this report the synthesis of novel zinc oxide (ZnO) with less defect density and its effect on Al/ZnO Schottky junction has been demonstrated. The defect density was estimated by positron annihilation lifetime measurement which ensures the material's superiority (i.e. free from point defects or any type of vacancies) over the earlier reported results. The thin film device of synthesized ZnO was fabricated on ITO coated glass substrate. As the front contact was made by aluminium, the characteristic I-V produced rectifying Schottky behavior. The underlying charge transport mechanism through metal-semiconductor (i.e. Al-ZnO) junction was analyzed on the basis of thermoionic emission theory to find out the quality of the fabricated device. In this regard we have studied the charge transport mechanism by measuring the density of states (DOS) at Fermi level, mobility-lifetime product and diffusion length.

Keywords: Zinc oxide; Positron annihilation spectroscopy; Defects; Transport property; Schottky diode.

1. Introduction

Zinc oxide (ZnO) nanoparticles are being extensively studied due to their unique electronic and optical properties. ZnO has wide range of technological applications which include sensors [1], transparent electrodes [2], Schottky diodes [3], solar cells [4] and piezoelectric devices [5]. Regardless of these advantages, it should be noted that ZnO is a defect rich material due to its large surface area in nanoscale regime. These defects play an important role in magnetic, chemical and physical properties. Defects may influence the charge transport property through material as well as in junctions or can affect the interfacial electrical properties [6]. So, for the better performance of Schottky diode, less defective material is desired. In this work, we have synthesized less defective ZnO nanoparticles and analyzed its effect on device performance.

Till date, several techniques including chemical synthesis, sol-gel technique [7], spray pyrolysis [8], hydrothermal technique [3], etc. have been adopted to synthesize ZnO nanoparticles of different morphology. Among these, the hydrothermal method has the advantages of low cost, controlled chemical growth of the sample, and can be implemented in a standard laboratory.

The occurrence of various types of material defects, such as Zn vacancy (V_{Zn}), Zn interstitial (I_{Zn}), void, cluster defects, triple junction defects [9, 10] in ZnO nanomaterial, depending upon synthesis techniques have been investigated. Defects or vacancies are directly related to the variation of electron density at the defects site. These defects coarsely influence the various junctions in electronic devices which eventually deteriorate the performance of the Schottky diodes by increasing the rate of recombination [11].

In this article the defect density of hydrothermally synthesized ZnO nanoparticles was estimated by the analysis of positron annihilation lifetime measurement. Its superiority was verified by comparing the obtained value with the earlier reported data. With this ZnO, Al/ZnO based Schottky junction was fabricated on ITO coated glass substrate. The charge-transportation mechanism within the device was analyzed by space-charge-limited-current (SCLC) theory. The diffusion length (L_D), mobility life-time ($\mu\tau$) product and density of states (DOS) at Fermi level were estimated analytically to get detail about the performance of the device. Moreover the

transport phenomena through the metal-semiconductor junction were also studied at different annealing temperature.

2. Materials and methods

In a typical synthesis of ZnO nanoparticles, 0.05 g of 1 mM anhydrous zinc nitrate was dissolved in 20 ml of de-ionized (DI) water by vigorous stirring at 70 ^{0}C temperature. Then it was diluted to 200 ml followed by cooling to room temperature. Separately prepared 100 ml of 0.02 M NaOH solution was added drop-wise to the mixture under rigorous stirring. A white precipitate (ppt) was obtained, which was transferred to a Teflon-lined stainless steel autoclave and heated at 160 ^{0}C for 48 hours. After cooling down to room temperature, ppt was washed with distilled water and ethanol repeatedly and sequentially to extract ZnO by centrifuge technique. Finally the synthesized material was collected as powder form by drying at 70 ^{0}C.

The structural, optical and electrical properties of synthesized material were characterized by Bruker D8 powder X-ray Diffractometer, FEI-Inspect F50 Field Emission Scanning Electron Microscope, Shimadzu 2401PC UV–vis spectrophotometer, Perkin Elmer LS-55 spectrofluorimeter and Keithley 2400 sourcemeter. The defect density of the sample was detected by positron annihilation lifetime measurements, which was carried out by using a fast-fast coincidence system consisting of two 1 inch tapered off BaF_2 scintillators coupled to XP 2020Q photomultiplier tubes. The time resolution (290 ps) was measured by using a ^{60}Co source with start and stop channel gates set at 1.27 and 0.511 MeV (prompt and annihilation gamma ray energies of ^{22}Na source) respectively. A 8 μCi ^{22}Na positron source (deposited on nickel foil) was used for lifetime measurements and spectra were fitted by the PATFIT 88 [12] programme after incorporating necessary source corrections.

To fabricate the Schottky diode of configuration ITO/ZnO/Al, the ITO coated glass substrate was cleaned with soap solution, acetone, ethanol, and distilled water by ultrasonication technique. The dispersed solution of ZnO nanoparticles in chloroform medium was prepared under sonication. It was spin coated on to pre-cleaned ITO substrate by spinning at 1600 rpm for 2 minutes and was dried at 100 ^{0}C inside a vacuum oven for 30 minutes. Aluminum was

deposited on thin film to prepare the metal-semiconductor interface by thermal evaporation technique, maintaining the effective diode area as 7.065×10^{-2} cm^2 with shadow mask.

Electrical characterization of the device was performed by recording the current-voltage (I-V) characteristics with the help of Keithley 2400 sourcemeter.

3. Results and Discussions

Fig. 1(a) represents the XRD pattern of the sample. The responsible peaks of corresponding (hkl) plane of the pattern approved the material as ZnO, which is supported by JCPDS card No: 79-2205. The XRD pattern illustrates that all the responsible peaks are broad and lower intensity, which indicates that the size of the crystal lattices are quite small. Williamson-Halls' estimation has been employed to measure the average grain size of the lattice-site. From the intercept of the extrapolated linear part of the curve $B_r \cos\theta$ vs. $\sin\theta$ (Fig. 1(b)) the particle size was found to be 15 nm whereas the FESEM image (Fig. 2) illustrates that the morphology of the nanoparticles are spherical in shape and ~ 40 nm to 45 nm in size. The lattice strain (μ) was also evaluated as 1.69×10^{-3} from the slope of fitted straight-line by considering the Williamson-Hall equation:

$$\mathbf{B_r \cos\theta = \frac{K\lambda}{D} + \mu \sin\theta} \qquad (1)$$

To find out the defects (as well as the density of electron at the annihilation site) within the synthesized material, the positron annihilation lifetime analysis had been performed. In defect rich ZnO nanomaterial, there are various types of defects, such as Zn vacancy (V_{Zn}), Zn interstitial (I_{Zn}), void, cluster defects and triple junction defects [10]. At the defect site, electron density is lower than that in the bulk of the material and lifetime of positrons is more than that of a defect free sample. Most of the positrons get trapped in the vicinity of grain boundaries as they are rich in defects and act as strong trapping centers for positrons. So, positron lifetime spectra provide information regarding the annihilation at grain boundaries only. According to the different defect size, the positron lifetime spectra of the ZnO nanoparticles were deconvoluted with three lifetime components, τ_1, τ_2 and τ_3 with their relative intensities I_1, I_2 and I_3, respectively. The shortest lifetime τ_1 represents the positron annihilation at structural defects in

the grain boundaries. Oxygen vacancy is not sensed by positron due to their appearance in neutral charge states. Only cation vacancy is visible to positrons. So, τ_1 indicates the presence of V_{Zn} clusters or vacancy at grain boundaries. The intermediate lifetime τ_2 may be due to divacancy or trapping of positrons in nanovoids at the intersection of three or more grain boundaries (e.g., triple junction). The last longer lifetime τ_3 is attributed to the pick-off annihilation of orthopositronium formed in the intercrystalline regions. The lifetime τ_3 is characterized by a large free volume present in the samples. Since intensity of the third lifetime component is very low (~0.06 %) compared to others, the first two lifetime components are only discussed. Fig-3 shows the positron annihilation lifetime spectra of as synthesized sample.

In our sample, shortest lifetime component (τ_1) value was found to be 160 ±7 ps with corresponding lifetime intensity (I_1) as 32.31±2.05 %. This obtained τ_1 value is very close to the reported positron lifetime value for defect free bulk ZnO [13]. It signifies that our sample is free from any type of cationic monovacancies (i.e. V_{Zn}, I_{Zn}, etc.) or smaller surface defects. This lifetime component has also occurred due to only free annihilation at the grain boundaries. The sample preparation was performed in a controlled way (pH and salt ratio) to reduce the defects in ZnO nanocrystals and interestingly we obtained more or less the same value of τ_1 in our sample compared to the reported defect free bulk ZnO [13]. On the other hand, since for this sample τ_1 value is much smaller than the earlier reported values [9- 11], we can infer that our sample posses very less cationic vacancy and the corresponding I_1 is due to only free annihilation without any monovacancies. The intermediate lifetime (τ_2) value for our sample is found to be 324 ±3 ps, which is far greater than the reported lifetime value of monovacancy in ZnO (~237 ps) [14] and obviously it should be lower than positron lifetime value of divacancies or vacancy cluster which may be formed in nanocrystalline ZnO. The Obtained value of τ_2 indicates that the intermediate lifetime originates due to positron annihilation with the free volume present inside the nanocrystalline grains. This implies that the main contributory factor is free spaces at the triple junction points other than divacancies or vacancy clusters. These values of lifetime components i.e. defect size of our ZnO nanocrystalline sample is much smaller than the earlier reported results [9- 11]. In nano-regime whenever the particle size decreases, volume at the triple junction point decreases and makes the sample compact. But at the same time intensity I_2 (67.63±2.04 %) is higher than I_1 (32.31±2.05 %) in our sample. This greater effect of I_2 is

attributed to the increase in number of triple junction point in the nano-regime. Presence of large number of nano-sized particles is responsible for this increase. Precisely, the more statistically reliable parameter is mean positron annihilation lifetime and it can be calculated as

$$\tau_m = \frac{(\tau_1 I_1 + \tau_2 I_2 + \tau_3 I_3)}{(I_1 + I_2 + I_3)} \qquad (2)$$

The obtained value of mean lifetime (τ_m~ 273 ps) for our synthesized sample is lower than the reported results [9-11], indicating the minimal presence of defect in synthesized sample. Ramanachalam et al. reported that applied bias can influence the defect lifetime in schottky application, while the characteristics bulk lifetime remains constant (within statistical error) [11]. Since our sample shows mainly bulk lifetime and some free volume between inter-grain regions other than any point defects or vacancies, this material can be used in application purpose. Also, by using trapping model, Ramanachalam et al. showed that only a single dominant defect (positron trap) can hamper the charge transport property in the material.

Inset of Fig. 4 represents the UV-vis absorption (solid) and emission spectra (dashed) of the synthesized ZnO. The absorption spectrum depicts strong UV absorption at ~ 373 nm of our synthesized ZnO. The photoluminescence of the ZnO exhibits different features. In this spectrum two UV emission peaks at ~ 412 nm and at ~ 437 nm were obtained. The strong peak comes from recombination of excitons, which has taken place due to the recombination of electrons in singly occupied oxygen vacancies with photoexcited hole [15] and the rest one comes from the defective states.

The optical band gap of the material was determined by the Tauc's equation:

$$\alpha = \frac{A.(h\gamma - E_g)^{1/2}}{h\gamma} \qquad (3)$$

Where 'α' is the absorption coefficient, 'E_g' is the band gap, and 'A' is a constant. The band gap was obtained as 3.37 eV by extrapolating the linear region near the onset in a plot of $(\alpha h\gamma)^2$ versus $h\gamma$.

To get insight into the electrical behavior, the room temperature electrical conductivity of the ZnO was measured as 2.32 x 10^{-6} Scm^{-1} by thin film technique. The thickness of the film was

measured (~20 μm) with the help of cross-sectional view of FESEM image (Fig. 5). Such value of electrical conductivity and wide optical band gap (3.37 eV) with higher excitation energy make the material as a selective one metal-oxide semiconductor for specific electronic applications. Moreover this synthesized ZnO has less amount of defect density. These functionalized behaviors of the synthesized ZnO led us to believe that it can improve the performance of metal-semiconductor junction as well as the electric transport property through the junction by minimizing the constraints of the Schottky device those are occurring due to material impurity. So we have incorporated this less defective ZnO within ITO and aluminium (Al) as sandwich structure and recorded the characteristic I-V within applied bias ±1V which is given in Fig. 6(a). This curve illustrates that the forward current of the device shows a nonlinear behavior while the reverse current increases slowly with bias voltage. This rectifying nature exhibits Schottky barrier effect. At room temperature the rectification current ratio (On/Off ratio) of the device is 66 at ±1 V.

For better realization of the charge transport mechanism within the device we have investigated the logarithmic curve of current vs. voltage plots (Fig. 6(b)). According to this plot, the device displays exponential behavior in region I (Fig. 6(b)) (in the voltage range 0 to +0.25 V) which can be attributed to thermionic emission. Region II (in the voltage range 0.25 to 1.0 V) obeys power law behavior ($I \alpha V^n$); where the transport mechanism is governed by space charge limited current (SCLC) and recombination.

The standard equation of thermoionic emission of Schottky diode illustrates the relation between reversed saturation current and the barrier potential as [16]:

$$\mathbf{I_0 = AA^*T^2 exp\left(\frac{-q\emptyset_B}{KT}\right)} \qquad (4)$$

Where, I_0, q, k, T, A, A^*, and Φ_B stand for the saturation current in reverse bias, electronic charge, Boltzmann constant, Kelvin temperature, the effective area, Richardson constant, and the barrier potential height respectively. The effective diode area was considered as 7.065×10^{-2} cm^2. To evaluate the Richardson constant for our sample, the temperature dependant current-voltage characteristics (Fig. 6(d)) were analyzed. It was estimated as 10.3×10^{-9} $Acm^{-2}K^{-2}$ by measuring the intercept of the extrapolated linear curve ln (I_0/T^2) vs. q/KT (Fig. 6(e)). Fig.

6(f) depicted the temperature dependant carrier mobility. The ideality factor (η) was determined as 0.38 from H (I) vs. I curve (Fig. 6(c)) by the formalism proposed by S. K. Cheung and N. W. Cheung:

$$\mathbf{H(I) = R_S I + \eta\eta\emptyset_b} \quad (5)$$

Where R_s is the series resistance and H(I) is defined as:

$$\mathbf{H(I) = V - \frac{\eta\eta KT}{q} ln(\frac{I}{AA^*T^2})} \quad (6)$$

The ideality factor for ideal Schottky diode is unity. In the present case, the ideality factor is smaller than unity. This deviation is probably due to multi generation-recombination via interface traps in the junction region [17]. This deviation of ideality factor indicates that the interface is not purely intimate metal-semiconductor but there must be some trapping states in interfacing layer [3], which can act as localized generation-recombination centers. The more disorderness in the structure of the nanoparticles increases the density of trapping states which affect the value of ideality factor. The occurrence of trapping states can be reduced by annealing the junction. That was confirmed by analyzing the I-V characteristics of the device at the temperature range 30 ^{0}C -150 ^{0}C with interval of 40 ^{0}C (Fig. 6(d), 7(a) and 7(b)). The important parameters of the Schottky diode were evaluated by proposed thermo-ionic emission theory and listed in Table I. From Table-I, it is obvious that the obtained schottky parameter are not giving rise to a new era in the performance of device. It might be attributed to the occurrence of various defects and interface states at the metal-semiconductor junction during the formation. In fact interface states are always introduced due to oxidation of semiconductor surfaces from extended air exposure, surface dipoles, incomplete covalent bonds, hydrogen and chemical reactions during fabrication processes and sharp discontinuity between semiconductor crystal and metal [18, 19].Such defects produce a large density of interface states which are continuously distributed in the energy within the forbidden gap and cause leakage currents to flow. These are the dominating effects for deterioration of device performance. Presence of bulk defects and oxygen vacancy at the junction may perturb the charge transportation. These defects cannot be sensed by positron. So the device performance not only depends upon the material property but

also the junction formation. To obtain the effective parameters we have investigated the carrier transport by intervening into the grain interior and the metal-semiconductor interface.

To get better insight of the device interface and charge transport phenomena, the effective carrier mobility at room temperature was found to be 7.3 x 10^4 $cm^2V^{-1}s^{-1}$ from logarithmic plot of current verses voltage (Fig. 6(b)) by evaluating the slope of region II with the help of Mott-Gurney space charge limited current (SCLC) equation [20]:

$$\mathbf{J} = \frac{\mathbf{9\mu_{eff}\in_0\in_r}}{\mathbf{8}}\left(\frac{\mathbf{V^2}}{\mathbf{d^3}}\right) \quad (7)$$

Where, J is the current density, ε_0 is the permittivity of free space, ε_r is the relative dielectric constant. The literature value of ε_r=2.9 for metal oxide semiconductor nanoparticles was employed [3]. Moreover we have studied the effect of temperature on the carrier mobility. We have encountered all the characteristic curves at different temperatures (Fig. 6(d), 7(a), 7(b)) and listed the values in Table I.

Fig.6 (f) illustrates that the carrier mobility was increased with the increase in temperature. The performance of the device not only can be understood by analyzing the carrier mobility data but also by analyzing the density of states (DOS) at the Fermi level. The DOS at Fermi level was determined from the SCLC region of current-voltage characteristics of different temperature (ranging from 30 ^{0}C -150 ^{0}C) with the help of equation [21]:

$$\mathbf{N'(E_F)} = \frac{\mathbf{2\in_r\in_0\Delta V}}{\mathbf{qd^2\Delta E_F}} \quad (8)$$

where E_F is the quasi-Fermi level, was estimated by the equation:

$$\mathbf{\Delta E_F = KTln\left(\frac{I_2V_1}{I_2V_1}\right)} \quad (9)$$

where V_1 and V_2 are different voltages in the space charge region (Fig. 6(d)). From the slope of SCLC region of characteristic I-V plot (Fig. 6(d)) for the bias potential, the transient time (τ) of the charge carrier was estimated with the help of the equation:

$$\boldsymbol{\tau} = \frac{\mathbf{9\in_0\in_r}}{\mathbf{8d}}\left(\frac{\mathbf{V}}{\mathbf{J}}\right) \quad (10)$$

here, d is the distance between two electrodes i.e. the thickness of the film (Fig. 5).

Moreover, to calculate the diffusion length of the charge carrier we have introduced Einstein-Smoluchowski equation:

$$\mu = \frac{qD}{K_B T} \quad (11)$$

Where, 'D' is the diffusion coefficient which depends on purity of the material and 'T' is the temperature in Kelvin scale. By using the above equation, values of 'D' were estimated. Hence the L_D was estimated by substituting 'D' value in equation:

$$L_D = \sqrt{2D\tau} \quad (12)$$

Results are tabulated in Table I. which shows that the value of DOS at Fermi level is quite higher than the earlier reports [22]. The accumulation of higher number of DOS at Fermi level increases the number of trapping states, which also degrades the performance of the metal-semiconductor devices. Here the DOS at Fermi level decreased as the temperature increased which is evitable for better performance. This implies the occurrence of less number of localized generation-recombination centers which improves the performance of the device and the rectification ratio. The rectification of current highly depends on carrier diffusion length (L_D) and mobility-lifetime ($\mu\tau$) product of the charge carriers. The effect of annealing on L_D and $\mu\tau$ can be realized from Fig. 8(a)-8(d). These figures illustrate that the mobility of the carriers has been improved as the temperature of the device is increased (Fig. 8(a)), whereas the transient time of the carriers inside the device decreased accordingly (Fig. 8(b)). There is a trade-off between carrier mobility and transient time, which are governed by the purity of the material. The ultimate performance of the device depends on mobility lifetime ($\mu\tau$) product and diffusion length (L_D), which of course depends on the defected level of the semiconductor material. In this analysis both of these quantities improved with the increase in temperature (Fig. 8(c) and (d)) and finally improves the performance of the device.

The magnitudes of the measured values are listed in Table I. From which it is very much clear that depending upon the temperature of annealing, the device performance indicating parameters like DOS at Fermi level, diffusion length (L_D) and the mobility-life time product ($\mu\tau$)

were improved. The estimated value of carrier mobility and space-charge-density supported the occurrence of trapping states, which is highly controlled by the regular/irregular structure of the junction and the occurrence of defect in the formation of metal-semiconductor interface rather than the defect in material. With the increase of annealing temperature, metal-semiconductor junction becomes more regular and the density of grain-boundaries is reduced, which can effectively improve the performance of Schottky junction diode. So by optimizing the annealing temperature, the performance of ITO/ZnO/Al based device can be improved upto the mark with defect free ZnO. Thus to reduce the grain boundaries and trapping states at metal-semiconductor interface, this novel ZnO of regular structure can be selective one in fabrication of thin active Schottky diodes [23]. Nevertheless by optimizing the constraints of device, precisely the film, performance can be improved further by using this kind of less defective ZnO.

Conclusions

Here we have reported a novel type of nanostructured semiconducting ZnO material having less defect density which was estimated from positron annihilation lifetime data. We have successfully applied this ZnO in metal-semiconductor Schottky diode and analyzed the device performance. It was realized that the estimated device parameters such as On/Off current ratio, barrier potential, series resistance, DOS etc. never solely depends upon the defects present in material.

Although positron lifetime measurement ensures material's superiority, the device performance may depend upon the junction properties which are controlled by the fabrication procedure.

Temperature dependent study proposed that the performance of the ITO/ZnO/Al based Schottky device could be improved further by optimizing the annealing temperature.

Acknowledgement

The authors acknowledge the support of PURSE and FIST program of DST, Government of India.

References

[1] C. H. Kwon, H. K. Hong, D. H. Yun, K. Lee, S. T. Kim, Y. H. Roh and B. H. Lee, *Sens. Actuators B*, 1995, 25, 610-613.

[2] S. Major, A. Banerjee, K. L. Chopra and K. C. Nagpal, *Thin Solid Films*,1986,143,19-30.

[3] S. Middya, A. Layek, A. Dey, J. Datta, M. Das, C. Banerjee and P. P. Ray, *Chem. Phys. Lett.*, 2014, 610-611, 39.

[4] S. Middya, A. Layek, A. Dey and P. P. Ray, *J Mater Sci: Mater Electron*, 2013, 24 (11), 4621-4629.

[5] J. G. E. Gardeniers, Z. M. Rittersma and G. J. Burger, *J. Appl. Phys*., 1998, 83, 7844.

[6] S. Lee, Y. Lee, D. Y. Kim and T. W. Kang, *Appl. Phys. Lett.*, 2010, 96, 142102.

[7] S. Rani, P. Suri, P. K. Shishodia and R. M. Mehra, *Sol Energy Mater Sol Cell*, 2008, 92, 1639-1645.

[8] R. Martins, R. Igreja, I. Ferreira, A. Marques, A. Pimentel, A. Gonçalves and E. Fortunato, *Mater Sci Eng B*, 2005, 118, 135-140.

[9] A. Roychowdhury, S. P. Pati, A. K. Mishra, S. Kumar and D. Das, *J. Phys. Chem. Solids*, 2013,74, 811-818.

[10] A. K. Mishra, S. K. Chaudhuri, S. Mukherjee, A. Priyam, A. Saha and D. Das, *J. Appl. Phys.*, 2007, 102, 103514.

[11] M. S. Ramanachalam, A. Rohtagi, J. P. Schaffer, T. K. Gupta, *J. Appl. Phys*., 1991, 69, 8380.

[12] P. Kirkegaard, M. Eldrup, *Comput. Phys. Comm*., 1972, 3, 240.

[13] Z. Q. Chen, S. Yamamoto, M. Maekawa, A. Kawasuso, X. L. Yuan and T. Sekiguchi, *J. Appl. Phys.*, 2003, 94, 4807.

[14] F. Tuomisto, V. Ranki, K. Saarinen and D. C. Look, *Phys. Rev. Lett.*, 2003, 91, 205502: 1-4.

[15] J. Zhang, L. Sun, J. Yin, H. Su, C. Liao and C. Yan, *Chem. Mater*., 2002, 14, 4172-4177.

[16] S. M. Sze, Physics of semiconductor devices, Wiley, New York, 1979.

[17] M. Campos, L. O. S. Bulhoes and C. A. Lindino, *Sens. Actuators*, 2000, 87 (1-2), 67-71.

[18] B. G. Streetman and S. K. Banerjee, Solid State Electronic Devices, 6th edn, Englewood Cliffs, NJ: Prentice-Hall, 2006.

[19] L. J. Brillson, *J. Phys. Chem. Solids,* 1983, 44, 703.

[20] P. W. M. Blom, M. J. M. de Jong and M. G. van Munster, Phys. Rev. B: Condens. Matter., 1997, 55(2), R656-R659.

[21] B. Gan, J. Ahn. Rusli, Q. Zhang, S. F. Yoon, V. A. Ligatchev, J. Yu, K. Chew and Q. F. Huang, *J. Appl. Phys.*, 2001, 89 (10), 5747-5753.

[22] Dhananjay, J. Nagaraju and S.B. Krupanidhi, *Physica B*, 2007, 391, 344-349.

[23] J. Sworakowski and J. Ulanski, *Annu. Rep. Prog. Chem. Sect. C*, 2003, 99, 87-125.

Figure captions:

Fig. 1: (a) XRD spectra of ZnO; **(b)** Williamson-Hall plot

Fig. 2: SEM image of ZnO

Fig. 3: Positron Annihilation spectra of Synthesized ZnO

Fig. 4: Tauc's plot; **Inset:** UV-absorption and PL emission spectra

Fig. 5: Cross sectional SEM image of the ZnO film on ITO

Fig. 6 (a): Current- Voltage characteristic at room temperature with semilogarithmic plot of I vs V at inset; **(b):** logarithmic plot of I vs. V at room temperature; **(c):** H(I) vs. I plot for the temperature 303K; **(d):** I –V characteristics at temperature 303K, 343K, 383K, and 423K; **(e):**

$\ln(I_0/T^2)$ vs. q/KT plot at temperature 303K, 343K, 383K, and 423K; **(f):** Temperature dependant carrier mobility graph.

Fig. 7(a): ln(I) vs. ln(V) plot of the Schottky diode at temperatures 303K, 343K, 383K, and 423K; **(b):** H(I) vs. I plots of the device at temperature 303K, 343K, 383K, and 423K

Fig. 8(a): Carrier mobility vs. temperature graph; **(b):** Life-time vs. temperature graph; **(c):** mobility-lifetime vs. temperature graph and **(d):** L_D vs. temperature graph

Table Captions:

Table I: Characteristic parameters of Schottky diode at different temperature

Fig. 1

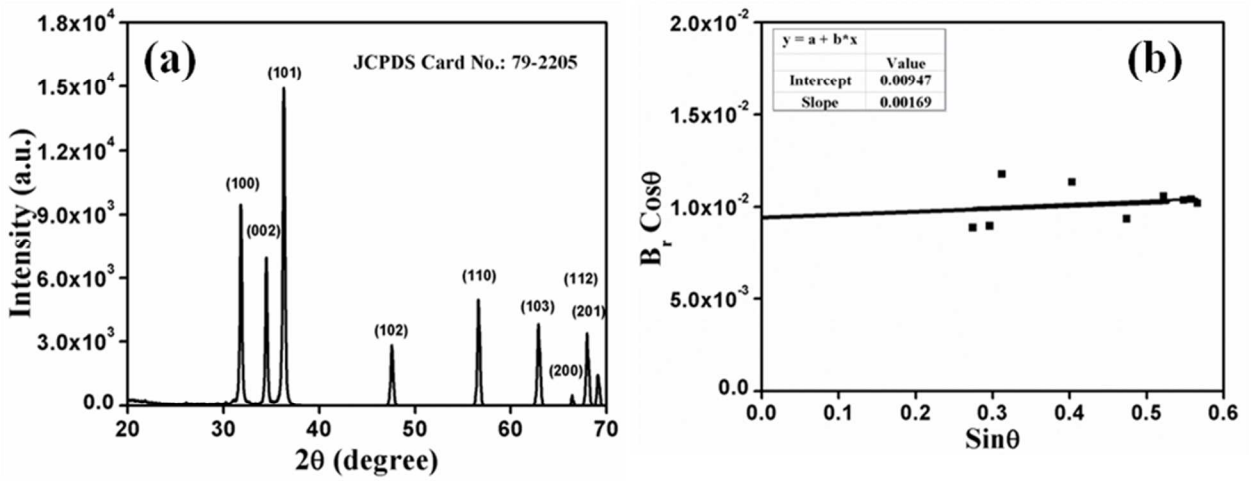

Fig. 2

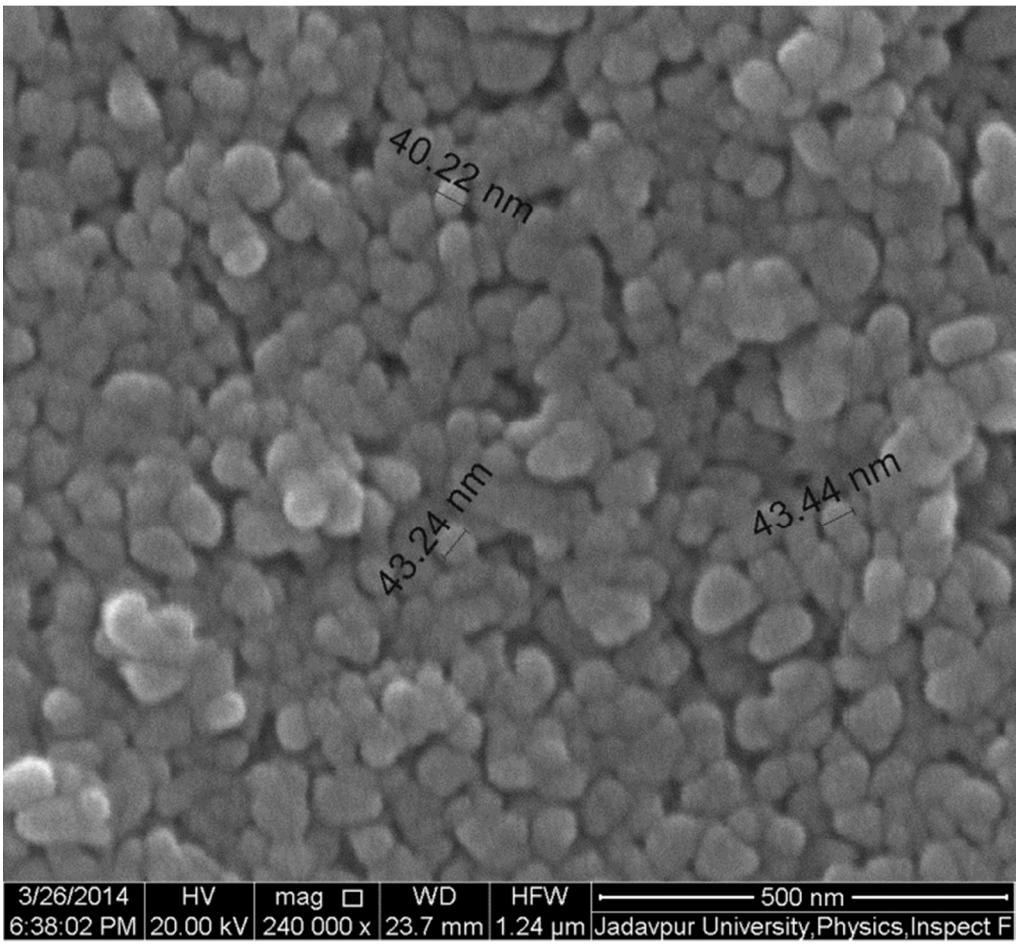

Fig. 3

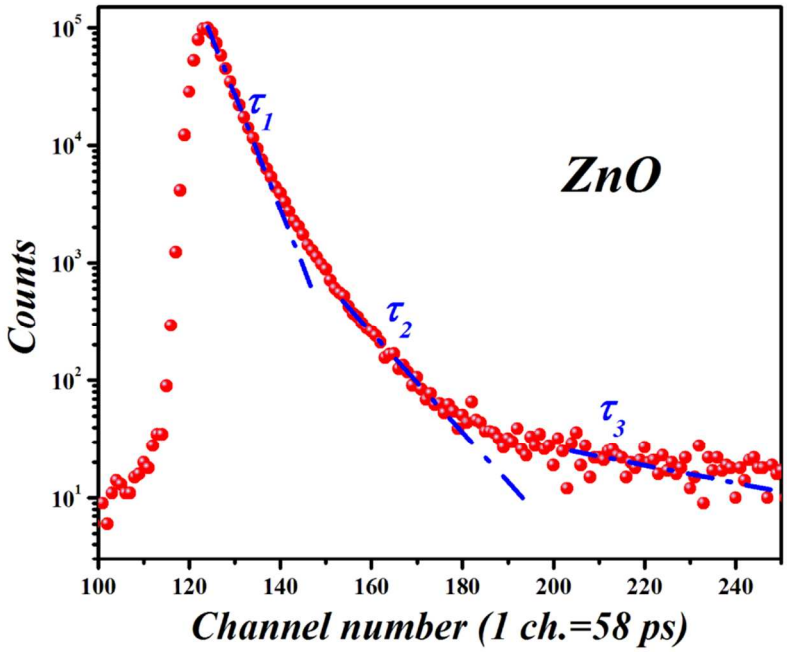

Fig. 4

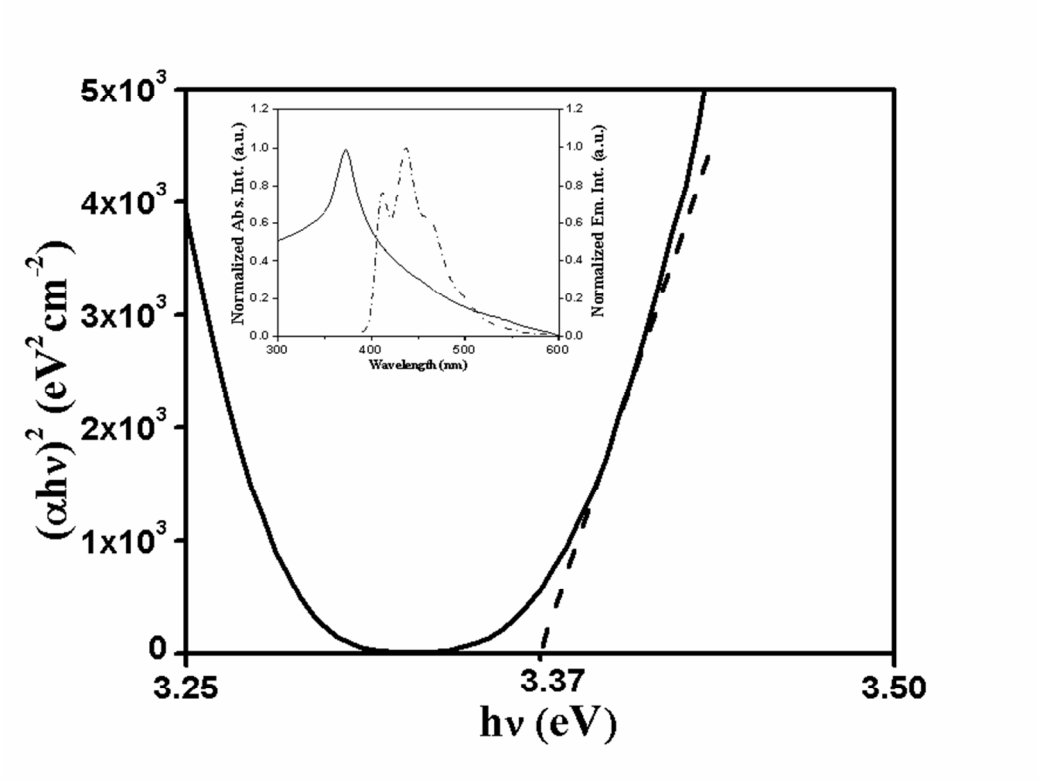

Fig. 5

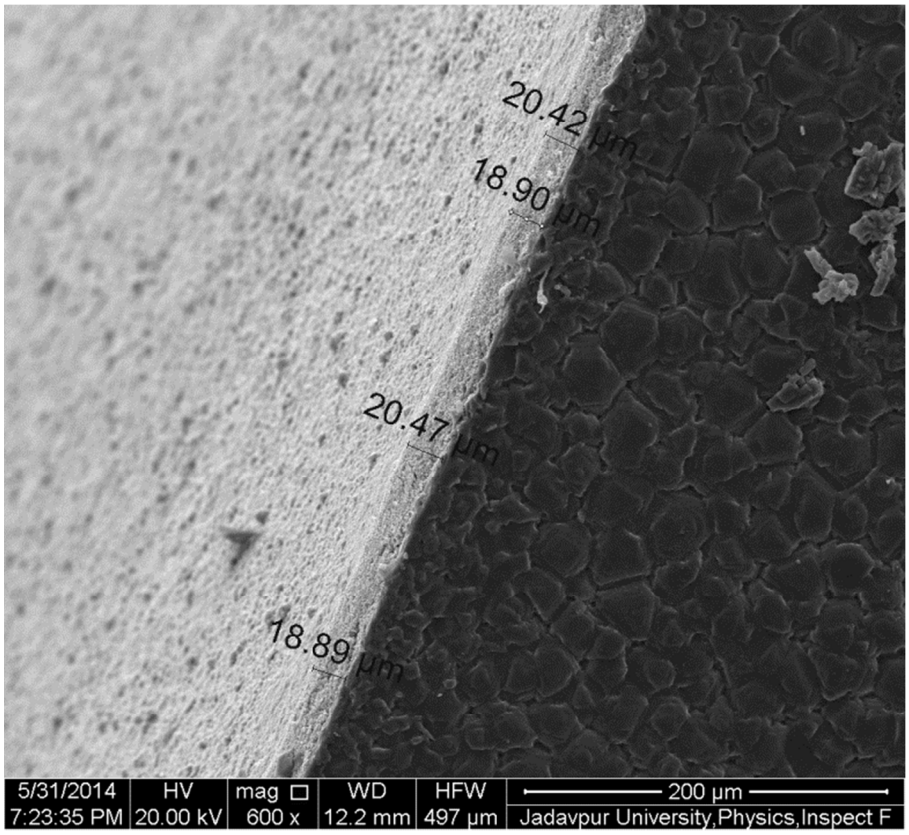

Fig. 6

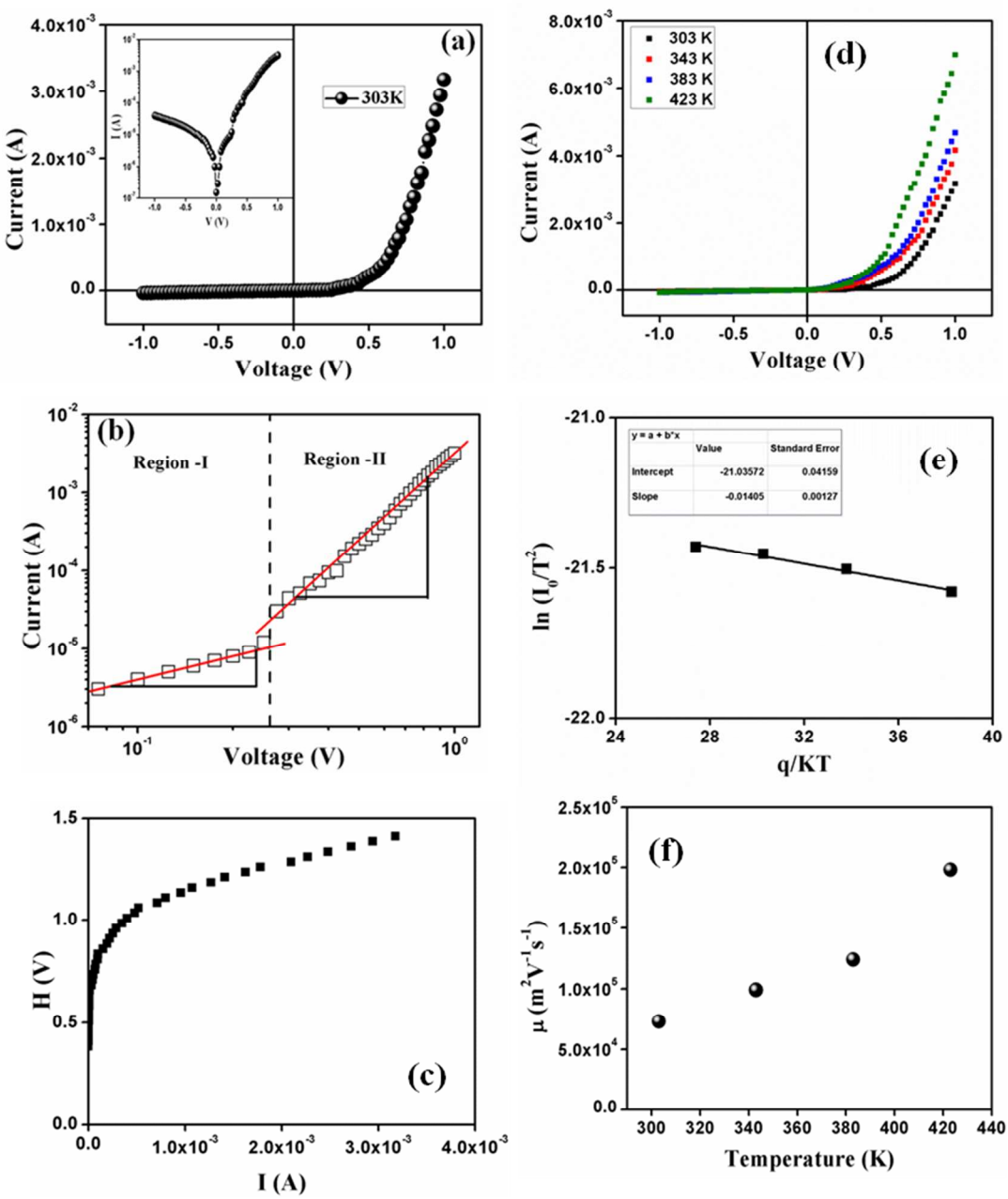

Fig. 7

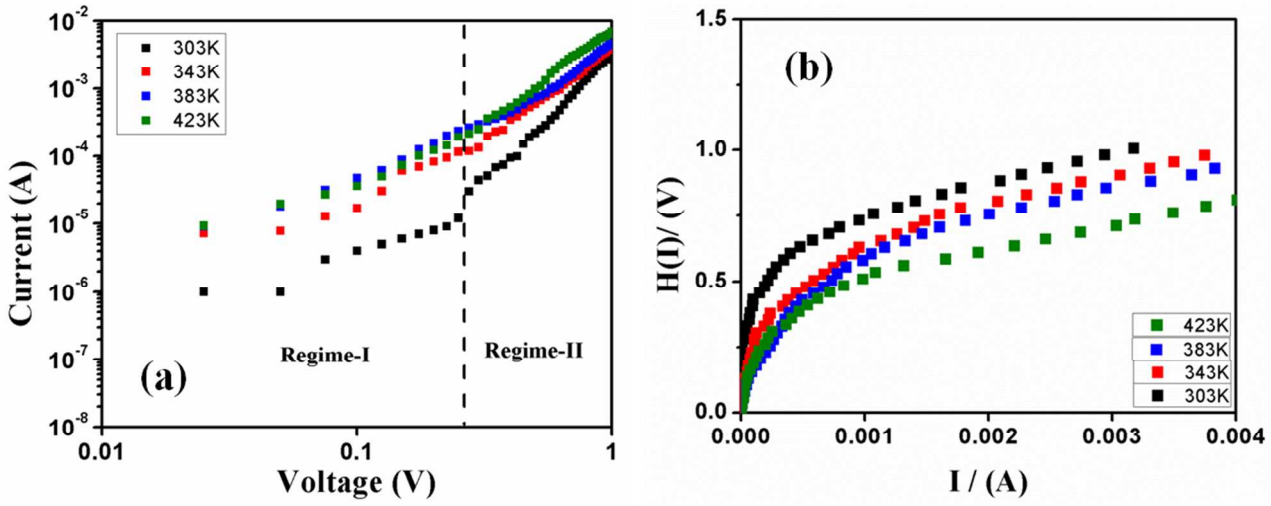

Fig. 8

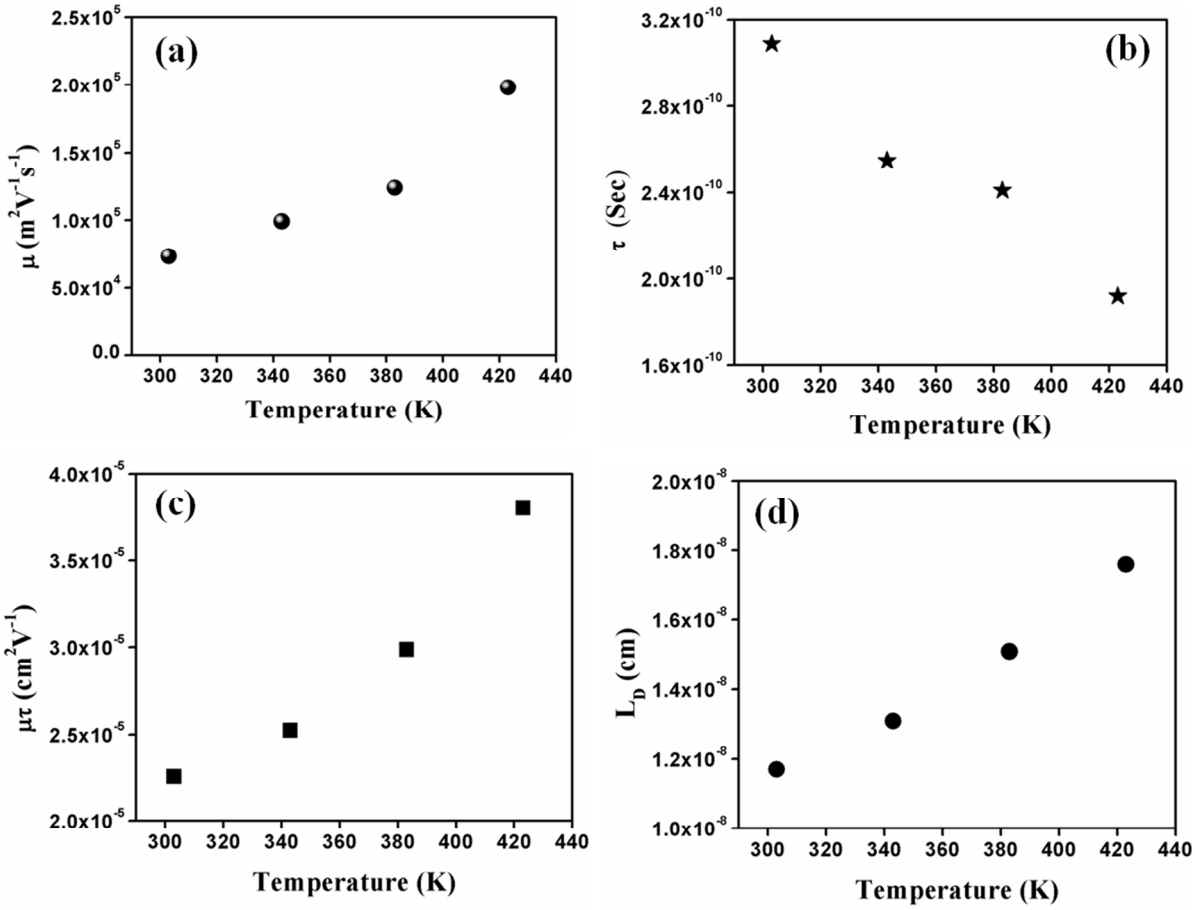

Table I

Temperature	n	On/Off	$Ø_b$ (eV)	(μ_{eff}) x10^4 ($cm^2V^{-1}s^{-1}$)	(τ) x10^{-11} (s)	($\mu\tau$) x10^{-5} (cm^2V^{-1})	DOS (e/Vcm^3)	L_D (Å)
303K	0.38	66	0.57	7.3	30.9	2.25	7.41 x 10^{17}	1.17
343K	0.43	77	0.38	9.9	25.5	2.52	2.69 x 10^{17}	1.31
383K	0.48	81	0.46	12.4	24.1	2.98	1.16 x 10^{17}	1.51
423K	0.53	102	0.66	19.8	19.2	3.80	1.07 x 10^{17}	1.76